Hybrid Numerical Simulation of Fluid Flow and Light Distribution in a Bubble Column Photobioreactor

Christopher McHardy[1], Giovanni Luzi[2], Jose Rodriguez Agudo[2],
Antonio Delgado[2,3] and Cornelia Rauh[1,2,3]

[1]*Institute of Food Biotechnology and Food Process Engineering, Technische Universität Berlin, Königin-Luise Str. 22, Berlin, Germany*
[2]*Institute of Fluid Mechanics, FAU Campus Busan, University of Erlangen-Nuremberg, 618-230 Busan, Republic of Korea*
[3]*Institute of Fluid Mechanics, University of Erlangen-Nuremberg, Cauerstr. 4, Erlangen, Germany*

Keywords: Photobioreactor, Microalgae, Light-Matter Interaction, Computational Fluid Dynamics, Radiation Transport, Lattice Boltzmann, Hybrid Method.

Abstract: Cultivation of phototrophic microorganisms occurs often in closed photobioreactors (PBR). Thereby, the distribution of light inside PBR is a key factor for phototrophic growth and reactor productivity. To predict local light intensities, it is often assumed that the absorption rate is constant in space, and scattering by microorganisms is negligible. The present contribution aims to present a hybrid model to simulate fluid flow characteristics and its impact on light fields in a bubble column PBR. First, numerical simulations of bubble column flow have been performed. Afterwards, the computed local air volume fractions have been used to obtain local radiation characteristics of the gassed suspension, and polychromatic light fields were computed and compared to the optically homogeneous case.

1 INTRODUCTION

Phototrophic microorganisms are characterized by the ability to use light energy to drive their cellular metabolism by means of photosynthesis. By doing so, the energy of light is used for the conversion of carbon dioxide into biomass. The ability to accumulate huge amounts of proteins or triacylglycerides into the biomass makes phototrophs a promising option for sustainable production of food, feed and fuels (Williams and Laurens, 2010).

Technical cultivation of phototrophs commonly occurs in closed PBR. Since the rate of photosynthesis is directly linked to the light intensity a cell is exposed to (Williams and Laurens, 2010), the distribution of light inside PBR is a key factor for phototrophic growth and productivity. The distribution of light is primarily determined by the presence of microorganisms. Light is absorbed along the path and consequently intensity is attenuated. Thereby, the local rate of absorption is directly proportional to the density of cells in the culture suspension (Pilon et al. 2011). Moreover, anisotropic

scattering of light causes a major difficulty for an accurate prediction of local light intensities because of two reasons. First, the scattering characteristics of the microorganisms must be measured (directly or indirectly), which is already a non-trivial task (Dauchet et al., 2015; Kandilian et al., 2016). Second, the computation of scattering requires an adequate discretization of the light angular distribution (Hunter and Guo, 2015). Due to these difficulties, a common approach in bioengineering is to neglect scattering and approximate light propagation by Lambert Beer's law instead of solving the full Radiative Transfer Equation (RTE).

It is often assumed that cells are homogeneously distributed in a PBR, and consequently also the radiation characteristics of the suspension are assumed to show no spatial variance. However, in most PBR gassing occurs to supply carbon dioxide to the suspension, remove oxygen and provide energy for mixing of the liquid phase (Olivieri et al., 2014). Since the light absorption of gas bubbles is negligible, and their scattering characteristics deviate from those of phototrophic cells, the assumption of an optically homogeneous suspension does not hold anymore in presence of bubbles.

The present contribution aims at presenting a methodology for computing radiation fields in multiphase flows. It is based on the assumption that the radiation characteristics of a mixture can be obtained by superimposing those of single components. Therefore, the hydrodynamic characterization of a PBR is required, for which Computational Fluid Dynamics (CFD) is a suitable tool. Two dimensional numerical simulations of fluid flow inside bioreactors are among the firsts that have been performed, since they require a lower numerical effort. However, they were found to be highly grid dependent (Bech, 2005). Three dimensional unsteady simulations are more adequate to reproduce the real complex flow patterns of bubble column flows. Examples of numerical simulations of fluid flow in a cylindrical bioreactor are reported in literature (Pfleger and Becker, 2001; Lobaton et al., 2011), but the so called "non-drag forces" are absent in their model. In recent and more complete models lift, virtual mass, wall lubrication and turbulent dispersion forces have been considered, since they strongly affect the flow field (Masood and Delgado, 2014). More sophisticated models integrate CFD, light distribution and kinetics growth of algae cells. Combination of CFD with Lambert Beer law and Aiba model (Zhang et al., 2015), or with optical ray tracing simulations based on an empirical three-parametric model (Krujatz et al. 2015) are reported. In other contributions compartmental modelling approach and photosynthetic factory model (Nauha et al., 2013), considering also light directionality and day and night conditions (Nauha et al., 2013) are presented.

In the present contribution, first, the bubble column flow inside a cylindrical PBR is simulated. Next, the local radiation characteristics of the gassed turbid suspension are computed. The RTE is solved afterwards by means of a Lattice Boltzmann solver (McHardy et al., 2016).

2 THEORY

Here, the mathematical models of fluid flow and light distribution are presented. The Eulerian-Eulerian formulation of two-phase flow and the applied Lattice Boltzmann method are described in detail.

2.1 Fluid Flow Model

An Eulerian-Eulerian approach is chosen to simulate the bubble column flow. Both, the continuous and the disperse phase are modelled as an interpenetrated continuum, where the inter-phase forces are taken into account by an extra term in the momentum equation. The corresponding mass conservation equations, both for the liquid and the gas phase read

$$\frac{\partial}{\partial t}\left(\rho_k \alpha_k\right) + \nabla \cdot \left(\rho_k \alpha_k \boldsymbol{u}_k\right) = 0 \tag{1}$$

where $k = L, G$. Here, L stands for liquid and G for gas. The other symbols $\boldsymbol{u}_k$, α_k and ρ_k denote the velocity vector, the volume fraction and the density of each phase, respectively. The momentum equations are

$$\frac{\partial}{\partial t}\left(\rho_k \alpha_k \boldsymbol{u}_k\right) + \nabla \cdot \left(\rho_k \alpha_k \boldsymbol{u}_k \boldsymbol{u}_k\right) = -\alpha_k \nabla p + \nabla \cdot \left(\alpha_k \boldsymbol{\tau}_k\right) + \rho_k \alpha_k \boldsymbol{g} + \boldsymbol{M}_{s,k} \tag{2}$$

where $s = L, G$. The terms on the left-hand side represent the temporal and convective acceleration, while those on the right-hand side represent the pressure gradient, the turbulent stress tensor, gravity and interphase forces (Masood and Delgado, 2014). The stress tensor is defined as

$$\boldsymbol{\tau}_k = \mu_{k,eff}\left[\nabla \boldsymbol{u}_k + \left(\nabla \boldsymbol{u}_k\right)^T\right] \tag{3}$$

where incompressibility has been assumed for both phases. The effective viscosity for each phase is the sum of the molecular and the turbulent one

$$\mu_{k,eff} = \mu_{k,Lam} + \mu_{k,Turb} \tag{4}$$

Finally, the last term of Eq. (2) reads

$$\boldsymbol{M}_{s,k} = \boldsymbol{M}_{L,G} = \sum_A \boldsymbol{F}_{L,G}^A = \boldsymbol{F}_{L,G}^D + \boldsymbol{F}_{L,G}^L + \boldsymbol{F}_{L,G}^{VM} + \boldsymbol{F}_{L,G}^{WL} + \boldsymbol{F}_{L,G}^{TD} = -\boldsymbol{M}_{G,L} \tag{5}$$

where the terms on right hand side of Eq. (5) are the drag, the lift, the virtual mass, the wall lubrication and the turbulent dispersion forces (Masood and Delgado, 2014). The drag force is due to viscous shear stress and pressure distribution around the bubble surface

$$\boldsymbol{F}_{L,G}^D = \frac{3}{4}\alpha_G \rho_L \frac{C_D}{d_B}\left|\boldsymbol{u}_G - \boldsymbol{u}_L\right|\left(\boldsymbol{u}_G - \boldsymbol{u}_L\right) \tag{6}$$

where C_D is the drag force coefficient and d_B is the bubble diameter. The Grace correlation is used to model C_D (Grace et al., 1976). The lift force acting on the gas phase due to a rotational liquid phase can be written as

$$\boldsymbol{F}_{L,G}^{L} = \alpha_G \rho_L C_L \left(\boldsymbol{u}_G - \boldsymbol{u}_L \right) \times \nabla \times \boldsymbol{u}_L \tag{7}$$

where C_L is computed according to the Legendre Magnaudet model (Legendre et al., 1998). The virtual mass force represents the added inertia to gas bubbles since they are moving through the liquid phase

$$\boldsymbol{F}_{L,G}^{VM} = \alpha_G \rho_L C_{VM} \left(\frac{\mathrm{D}\boldsymbol{u}_G}{\mathrm{D}t} - \frac{\mathrm{D}\boldsymbol{u}_L}{\mathrm{D}t} \right) \tag{8}$$

where $C_{VM} = 0.5$ is the virtual mass coefficient. The wall lubrication force is an artificial force that models the situation where bubbles concentrate in a region close to a wall

$$\boldsymbol{F}_{L,G}^{WL} = C_{WL} \alpha_G \rho_L \left| \boldsymbol{u}_L - \boldsymbol{u}_G \right|^2 \hat{\boldsymbol{n}}_W \tag{9}$$

where $\hat{\boldsymbol{n}}_W$ is the normal to a reactor surface and the coefficient C_{VM} is computed with the Frank model (Frank et al., 2004; Frank et al., 2008). Finally, the turbulent dispersion force is responsible for the dispersion of phases and it can be expressed as

$$\boldsymbol{F}_{L,G}^{TD} = C_{TD} C_D \frac{\nu_{L,Turb}}{\sigma_{L,Turb}} \left(\frac{\nabla \alpha_L}{\alpha_L} - \frac{\nabla \alpha_G}{\alpha_G} \right) \tag{10}$$

according to the Favre averaged model (Burns et al., 2004). Here, $\sigma_{L,Turb}$ is the turbulent Schmidt number for the continuous phase, and $C_{TD} = 1$ is a multiplier.

2.1.1 Turbulence Model

A two-equation model is able to accurately compute the turbulent viscosity of the continuous phase

$$\mu_{L,Turb} = \rho_L \frac{k}{\omega} \tag{11}$$

where k is the turbulent kinetic energy and ω is the turbulent frequency. These two quantities are here computed according to the Shear Stress Transport (SST) model (Menter, 1994) by solving two

independent scalar transport equations for k and for ω. A simple algebraic turbulence model is chosen for the gas phase

$$\mu_{G,Turb} = \frac{\rho_G}{\rho_L} \frac{\mu_{L,Turb}}{\sigma_{L,Turb}} \tag{12}$$

2.2 Radiative Transport Model

The RTE is a Boltzmann-type transport equation, which balances the spatio-temporal evolution of intensity of radiation (or radiance) $I\left(\boldsymbol{x}, \hat{\boldsymbol{s}}, t \right)$.

$$\frac{\partial I\left(\boldsymbol{x}, \hat{\boldsymbol{s}}, t \right)}{c \partial t} + \hat{\boldsymbol{s}} \cdot \nabla I\left(\boldsymbol{x}, \hat{\boldsymbol{s}}, t \right) = $$
$$\beta \left(-I\left(\boldsymbol{x}, \hat{\boldsymbol{s}}, t \right) + \frac{\omega}{4\pi} \int_{4\pi} I\left(\boldsymbol{x}, \hat{\boldsymbol{s}}', t \right) \Phi\left(\hat{\boldsymbol{s}}', \hat{\boldsymbol{s}} \right) \mathrm{d}\Omega \right) \tag{13}$$

In Eq. (13), c, t, Ω, β, $\hat{\boldsymbol{s}}$ and $\boldsymbol{x}$ denote speed of light, time, solid angle, extinction coefficient, unit direction and position vector. The scattering albedo ω_{sca} is defined as

$$\omega_{sca} = \frac{\sigma}{\sigma + \kappa} \tag{14}$$

where κ and σ denote the absorption and scattering coefficients, which are related to the extinction coefficient by $\beta = \kappa + \sigma$. Φ is the scattering phase function, which describes the angular distribution of scattered light. In Eq. (13), the emission of radiation by microorganisms is neglected, due to its minor relevance for the light field in photobioreactors. Properties of the RTE are described in detail elsewhere (Modest, 2013) and need not to be repeated here.

2.2.1 Radiation Transport Lattice Boltzmann Method (RT-LBM)

To solve Eq. (13), a lattice Boltzmann method (McHardy et al., 2016) is applied in this work. Following the usual lattice Boltzmann formalism, a discrete representation of Eq. (13) reads

$$I_{\lambda,i}\left(\boldsymbol{x} + \Delta \boldsymbol{x}, t + \Delta t \right) - I_{\lambda,i}\left(\boldsymbol{x}, t \right)$$
$$= -\mu_i \left(I_{\lambda,i}\left(\boldsymbol{x}, t \right) - I_{\lambda,i}^{eq}\left(\boldsymbol{x}, t \right) \right) \tag{15}$$

Herein, $I_{\lambda,i}$ is discretized in the momentum space, which consists of directional and frequency components. Therefore, a monochromatic radiation propagating along a trajectory, which is given by the connection of two nodes in a cubic lattice, is considered. The scattering from the jth into the ith trajectory is captured by the function $I_{\lambda,i}^{eq}(\boldsymbol{x},t)$, which is a discrete representation of the in-scattering integral in Eq. (13).

$$I_{\lambda,i}^{eq}(\boldsymbol{x},t) = \omega_\lambda w_i \sum_{j=1}^{Q} I_{\lambda,j}(\boldsymbol{x},t)\Phi_{i,j}f_{i,j} \qquad (16)$$

Thereby, the integral is replaced by a summation and the scattering phase function is represented by a symmetric Q by Q matrix which is computed by means of an algebraic method, proposed in (McHardy et al., 2016). A correction function $f_{i,j}$ considers that the propagation distance depends on the direction of propagation on a cubic lattice. The absorption and scattering coefficients may have spectral dependency, so ω_λ is also spectrally distributed. For a D3Q26 model (3 dimensions, 26 discrete trajectories), the nodes and weights w_i of the quadrature are shown in table 1. The quantity

$$\mu_{i,\lambda} = \beta_\lambda \Delta\boldsymbol{x}_i \qquad (17)$$

is the collision frequency and relates grid spacing to the mean free path of radiation. The collision frequency depends on direction, because the probability of collision increases with increasing path length.

The macroscopic quantities of the radiation field, namely mean intensity J and radiation flux $\boldsymbol{F}$, can be obtained by computing moments of $I_{\lambda,i}$.

$$J = \int \sum_{i=1}^{Q} w_i I_{\lambda,i} d\lambda \qquad (18a)$$

$$\boldsymbol{F} = \int \sum_{i=1}^{Q} \boldsymbol{c}_i w_i I_{\lambda,i} d\lambda \qquad (18b)$$

While the integration over solid angles is approximated by the summation over directions, the integration across the spectral component of momentum is approximated by composite Simpson's Rule, using a step length of $\Delta\lambda = 30$ nm.

Table 1: Lebedev quadrature on a unit sphere, used for discretization of the RTE. The nodes of the quadrature result from all possible permutations of the typical nodes.

i		typical node (x,y,z)	weights
1 -	6	(1,0,0)	1/21
7 -	14	1/√3 (1,1,1)	4/105
15 -	26	1/√2 (1,1,0)	9/280

2.2.2 Radiation Characteristics of Multiphase Suspensions

A major assumption of the presented methodology is that the radiation properties of a mixture can be obtained by superimposing those of the single components. This is true, if single particles scatter independently of each other. For suspensions of point-like scatterers, several criteria for estimating scattering-regimes can be found in literature. Baillis and Sacadura (2000) as well as Modest (2013) refer to a scattering regime map, which estimates the scattering regime with respect to the particle volume fraction and a size parameter. Jonasz and Fournier (2007) suggest as a criterion the relation $\beta\Delta x(1-g) \ll 1$, where g is the cosine of the mean scattering angle. For suspensions of microalgae at concentrations in the single-digit gram-per-litre range, typical for PBR, the suggested criteria are generally fulfilled. Therefore the radiation characteristics of a microalgae suspension can be obtained from

$$\kappa_A = c_A A_{ABS} \qquad (19a)$$

$$\sigma_A = c_A A_{SCA} \qquad (19b)$$

where c_A is the mass concentration of scatterers in the suspension and A is the mass-specific absorption or scattering cross-section, respectively.

For dispersed bubbles, the absorption and scattering coefficients can be computed analogously, by multiplying the number density of gas bubbles n_B by the absorption or scattering cross-section. It is assumed that bubble absorption is negligible compared to absorption by microalgae, therefore $\kappa_B = 0$. The number density of bubbles inside a control volume can be computed from the local air volume fraction and the volume of a single bubble V_B, in case of monodisperse bubbles. The scattering cross-section can be obtained by the geometrical

cross-section of a bubble A_B and the scattering efficiency Q_{sca}. Therefore, the scattering coefficient for dispersed bubbles becomes

$$\sigma_B(x) = \alpha_G(x)\frac{A_B Q_{sca}}{V_B} \tag{20}$$

In a gassed suspension of microalgae, the effects of the single components superimpose (Pilon et al., 2011; Berberoglu et al., 2007). The effective absorption and scattering coefficients of the mixture are given by

$$\kappa(x) = \kappa_A(1 - \alpha_G(x)) \tag{21a}$$

$$\sigma(x) = \sigma_A(1 - \alpha_G(x)) + \sigma_B \tag{21b}$$

In Eq. (21) it is considered that the liquid volume and therefore the volumetric concentration of microalgae are reduced by the presence of air. Since microalgae scatter light differently compared to gas bubbles, an effective scattering phase function must be computed. Pilon et al. (2011) suggests to use the scattering coefficients of microalgae and gas bubbles as weighting coefficients, so that the effective scattering phase function becomes

$$\Phi(x) = \frac{(1 - \alpha_G(x))\sigma_A \Phi_A + \sigma_B \Phi_B}{(1 - \alpha_G(x))\sigma_A + \sigma_B} \tag{22}$$

3 PHOTOBIOREACTOR MODEL

Here, details concerning simulation set-up are given. The physical parameters are described first, followed by the outline of geometry and grid generation, as well as numerical solutions of fluid flow and light distribution.

3.1 Physical Parameters

An isothermal cylindrical bubble column PBR of diameter $D = 9.4$ cm and height $H = 50$ cm with an air headspace of 10 cm is considered. The reactor is aerated from a small inlet of diameter $d = 4$ mm, located at the bottom of the column. Spherical monodisperse bubbles have a constant mean diameter $d_B = 7$ mm and mass flow rate $\dot{m}_G = 9.85 \cdot 10^{-6}$ kg/s. The PBR is illuminated by red LED from four sides. The spectrum of the LED is

approximated by a Gauss distribution with peak emission at 655 nm and 15 nm standard deviation.

A suspension of microalgae is located inside the PBR. The absorption and scattering cross-sections of the microalgae are assumed to be the same as measured by Kandilian et al. (2016) and cells are assumed to be present as individuals and no agglomeration occurs. Mie-scattering of cells is expressed by the Henyey-Greenstein phase function

$$\Phi = \frac{1}{4\pi}\frac{1 - g^2}{\left(1 + g^2 - 2g\cos(\theta)\right)^{1.5}} \tag{23}$$

where $g = 0.98$ (Kandilian et al., 2016). For gas bubbles, the asymmetry factor g_B was set to 0.86 and the scattering efficiency $Q_{sca} = 1$ was chosen as an approximation for Mie-scattering of large spheres (Pilon et al., 2011).

3.2 Fluid Flow Simulation

Both, the geometry and the grid have been created using the commercial software ANSYS ICEM®. The domain is covered with a structured mesh, obtained by using two O grids, and a mesh of 59059 volumes was selected. All numerical simulations were carried out using the commercial software ANSYS CFX® 15.0 which is a finite volume based solver. At the inlet, an air mass flow rate was set, and an opening boundary condition was set at the outlet. The remaining parts of the geometry have been set as walls, and a no slip condition for both air and water has been imposed.

Simulations with an air mass flow rate $\dot{m}_G = 4.85 \cdot 10^{-6}$ kg/s were run up to 60 s to initialize the flow field. A time step of $5 \cdot 10^{-4}$ s was chosen to advance the solution in time. Afterwards, the time step has been increased to 10^{-3} s, and the mass flow rate has been raised to the value of $\dot{m}_G = 9.85 \cdot 10^{-6}$ kg/s. Simulations have been run up to 140 s, the cut-off value of the residuals was set equal to 10^{-4} and a maximum number of thirty iterations for the inner cycle was imposed. The air volume fraction at every grid node has been extracted at the time step $t = 110$ s.

3.3 Simulation of Light Distribution

Solutions of the D3Q26 RT-LBM were computed in MATLAB®, using an in-house code. The computed local air-volume fractions were interpolated on a

lattice with 201 nodes along the column diameter. In total, the lattice was composed of approx. $1.16 \cdot 10^7$ nodes. The lattice was proven to produce converged solutions in a grid refinement study and is also used for computation in the RT-LBM.

At the side walls of the reactor parallel light enters the turbid suspension from four sides. Focussing of light by the curved reactor wall is not taken into account for the boundary modelling. It is assumed that the walls are non-reflective so that backscattered light can leave the computational domain. For each concentration of biomass c_A (0.6 g/L, 1.0 g/L), 7 monochromatic solutions were computed and integrated by means of Simpson's Rule to obtain the polychromatic solution. All parameters are shown in table 2. Achievement of steady-state in monochromatic simulations was estimated by introducing a relative error criterion.

$$\varepsilon = \max \left| 1 - \frac{I_{\lambda,i}\left(\boldsymbol{x}, t + \Delta t\right)}{I_{\lambda,i}\left(\boldsymbol{x}, t\right)} \right| \leq 10^{-6} \qquad (24)$$

Table 2: Spectral radiation characteristics of biomass and light source at the simulated wavelengths.

λ	[nm]	610	625	640	655
A_{abs}	[m²/kg]	136	156	176	259
A_{sca}	[m²/kg]	1628	1599	1538	1360
$I_{0,\lambda}/I_0$	1E-04 [-]	3	36	161	266

λ	[nm]	670	685	700
A_{abs}	[m²/kg]	358	311	70
A_{sca}	[m²/kg]	1139	1305	1941
$I_{0,\lambda}/I_0$	1E-04 [-]	161	36	3

4 RESULTS AND DISCUSSION

In this section, preliminary results are shown to demonstrate the applicability of the proposed hybrid methodology. It is shown how different biomass concentrations and presence of bubbles affect the light distribution inside a PBR. While the former has a strong impact on the intensity profile, the latter exhibits only a weak effect on it, probably due to the low mass flow rate used in this work.

4.1 Flow Field

Figure 1 shows a contour of air-volume fraction in a cross-sectional (x-y) plane at $z = 0$ at the time step

$t = 110$ s. It is an oscillating air bubble "plume", typical of an aerated bioreactor. The air volume fraction at each grid node is extracted at the selected time instant, so that optical properties of the suspension can be computed.
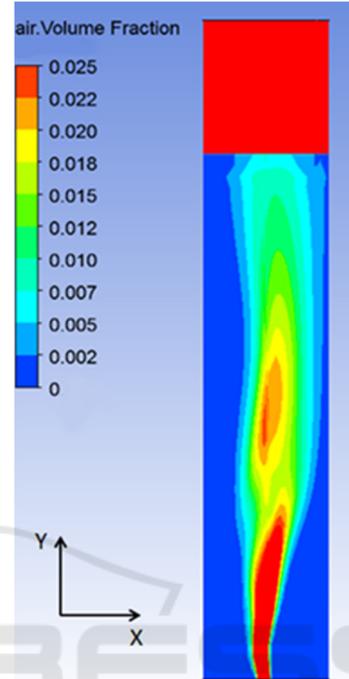

Figure 1: a) Air volume fraction on an x-y plane at $z = 0$ at the time instant $t = 110$ s. The mass flow rate is $\dot{m}_G = 9.85 \cdot 10^{-6}$ kg/s.

4.2 Radiation Field

The local air volume fractions were interpolated on a cubic lattice and grid independence was found for a grid resolution higher than 50 nodes along the column diameter (results not shown).

To evaluate the radiation field, profiles on the plane $y = 0.3$ m of the bubble column were computed. Figure 2 shows profiles of normalized monochromatic radiation at different wavelengths. Near the boundaries, the radiation emitted from different lamps overlap so that the magnitude of the normalized radiation field becomes greater than 1.

Figure 3 shows the polychromatic intensity profiles for two different concentrations of microalgae. For comparison, simulations of an optically homogeneous suspension (without gas) were performed. Although the profiles do not deviate much, slight differences (up to 6 %, not shown) were found in presence of gas.

Figure 4 shows the effect of gas bubbles on the light field more in detail. It can be seen that increase of biomass concentration damps the effect of the gas on the light field and biomass absorption becomes the dominant characteristic. However, the light field becomes asymmetric due to differences in local gas concentrations as it can be seen by comparing intensity profiles along the x- and z-axes or rather by the difference of the profiles (Dash-dotted and dotted lines in Figure 4).

Generally, the effect of gas bubbles on the light field is weak in the present case. However, the air volume fraction is higher at higher gas mass flow rates, and further investigations will address this effect. Moreover, the present study considers red LED lamps, which emit in the absorption maximum of microalgae (Williams and Laurens, 2010). It can be expected, that the effect of bubbles increases if light across the full visible spectrum is considered, due to the lower absorption in other spectral regions. Further model improvement will also consider the directional emission of light sources as well as focussing effects at the boundaries.

It is well known that flashing light has great potential to improve the productivity of PBR (Williams and Laurens, 2010). From a Lagrangian point of view, flashing light is realized if cells travel between bright and dark regions in the reactor. Investigations on this effect in PBR require transient simulations techniques, since optical accessibility and therefore experimental investigations are limited. The presented hybrid model offers the required functionality to investigate transient effects of the flow on the light field, and to trace virtual particles through the transient light field.
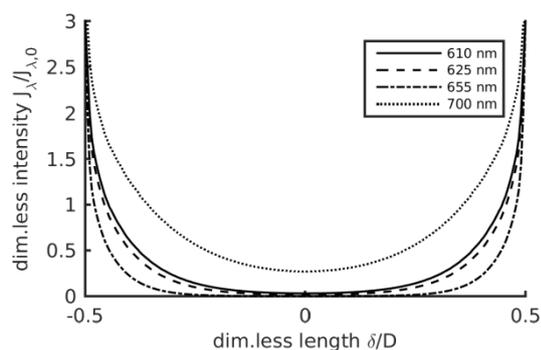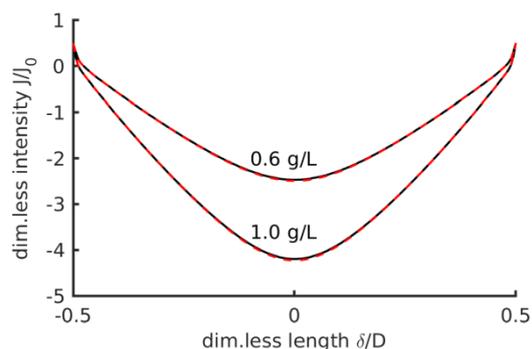

Figure 3: Profiles of polychromatic light intensity (log-scale) along the x-axis at $y = 0.3$ m and $z = 0$ in the PBR for different biomass concentrations with (solid lines) and without gas (dashed lines). δ is the radial coordinate.
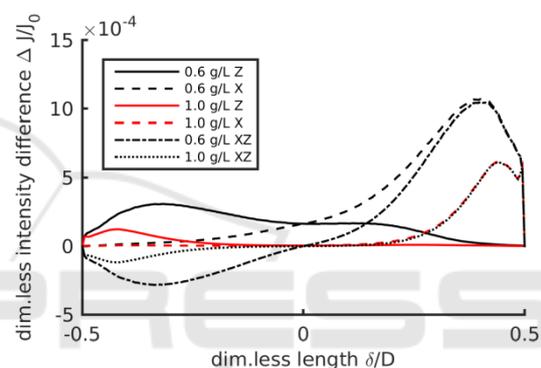

Figure 4: Effect of gas bubbles on light intensity. Solid and dashed lines compare the effect of gas bubbles to an optically homogeneous suspension at $y = 0.3$ m along the x- and z-axis, respectively. Dash-dotted and dotted lines show the difference of light intensity along x and z axis in the presence of gas bubbles. δ is the radial coordinate.

5 CONCLUSIONS

In this work a simulation framework was presented to couple fluid dynamics and radiation transfer. The method is innovative and no coupling of CFD and RT-LBM has been reported in literature before. This is, in particular, due to the fact that the development of RT-LBM is still a new field of research.

The methodology was applied to simulate flow and light fields in a bubble column PBR. Although the effect of gas bubbles on the light field was weak, further investigations will proof the generality of this result. To make use of the full power of the modelling framework, future work should also address transient impacts of gas bubbles on the light field to realize flashing-light regimes in PBR.

Figure 2: Profiles of monochromatic light intensity along the x-axis at $y = 0.3$ m and $z = 0$ in the PBR for $c_A = 0.6$ g/L. δ is the radial coordinate.

The link between CFD and RT-LBM was realized by computing local radiation properties from air-volume fractions and radiation properties of bubbles and single cells. If the cell density is not too high, the underlying assumption that radiation properties of a mixture can be obtained by superimposing those of single components remains valid. This enables to take local cell concentrations into account if mass transport of cells in incorporated into the CFD model. As shown by Dauchet et al. (2015), information as particle size distributions can also be considered for the calculation of radiation properties to obtain more realistic representative values, if desired. Similarly, it seems to be possible to treat mixtures of different cell species with different particle size.

REFERENCES

Baillis, D., Sacadura, J.-F., 2000. Thermal radiation properties of dispersed media: theoretical predication and experimental characterization. In *J. Quant. Spectrosc. Ra.*, 67(5): 327-363.

Bech, K., 2005. Dynamic simulation of a 2D bubble column. In *Chem. Ing. Sci.*, 60(19): 5294-5304.

Berberoglu, H., Yin, J., Pilon, L., 2007. Light transfer in bubble sparged photobioreactors for H_2 production and CO_2 mitigation. In *Int. J. Hydrogen Energ.*, 32(13): 2273-2285.

Burns, A.D.B., Frank, Th., Hamill, I., and Shi, J-M., 2004. The Favre Averaged Drag Model for Turbulent Dispersion in Eulerian Multi-Phase Flows. 5th International Conference on Multiphase Flow

Dauchet, J., Blanco, S., Cornet, J.-F., Fournier, R., 2015. Calculation of radiative properties of photosynthetic microorganisms. In *J. Quant. Spectrosc. Ra.*, 161: 60-84.

Frank, Th., Shi, J.M., Burns, A.D., 2004. Validation of Eulerian Multiphase Flow Models for Nuclear Safety Applications. In 3rd International Symposium on Two-Phase Flow Modelling and Experimentation, Pisa, Italy.

Frank, Th., Zwart, P.J., Krepper, E., Prasser, H.-M., Lucas, D., 2008. Validation of CFD models for mono- and polydisperse air-water two-phase flows in pipes. In *J. Nuclear Engineering & Design*, 238(3): 647–659.

Grace, J.R., Wairegi, T., Nguyen, T.H., 1976. Shapes and velocities of single drops and bubbles moving freely through immiscible liquids. In *Trans. Inst. Chem. Eng.*, 54 (3): 167-173.

Hunter, B., Guo, Z., 2015. Numerical smearing, ray effect, and angular false scattering in radiation transfer computation. *Int. J. Heat Mass Transfer*, 81: 63–74.

Jonasz, M., Fournier G.R.., 2007. *Light Scattering by Particles in Water,* Academic Press. Amsterdam, 1st edition.

Krujatz, F., Illing, R.·, Krautwer, T., Liao, J., Helbig K., Goy, K., Opitz, J., Cuniberti, G., Bley, T., Weber, J., 2015, Light-field-characterization in a continuous hydrogen-producing photobioreactor by optical simulation and computational fluid dynamics. In *Biotechnol Bioeng.*, 112(12): 2439-2449

Kandilian, R., Pruvost, J., Artu, A., Lemasson, C., Legrand, J., Pilon, L., 2016. Comparison of experimentally and theoretically determined radiation characteristics of photosynthetic microorganisms. In *J. Quant. Spectrosc. Ra.*, 175: 30-54.

Legendre, D., Magnaudet, J., 1998. The lift force on a spherical bubble in a viscous linear shear flow. In *J. Fluid Mech.,* 368: 81-126.

Lobaton, H.F.Q., Suarez, C.A., Molina, A., 2011. CFD-facilitated flow field analysis of bubble columns with concentric plates for biological applications. In *Chem. Eng. Technol.*, 34(9):1490-1496.

Masood, R.M.A., Delgado, A., 2014. Numerical investigation of the interphase forces and turbulence closure in 3D square bubble columns. In *Chem. Eng. Sci.*, 108(28), 154-168.

Menter, F.R., 1994. Two-equation eddy-viscosity turbulence models for engineering applications. In *AIAA Journal*, 32(8): 1598-1605.

McHardy, C., Horneber, T., Rauh, C., 2016. New lattice Boltzmann method for the simulation of three-dimensional radiation transfer in turbid media. In *Opt. Express*, 24(15): 16999-17017.

Modest M.F., 2013. *Radiative Heat Transfer*, Academic Press. Amsterdam, 3rd edition.

Nauha, E., K., Alopaeus, V. 2013. Modeling method for combining fluid dynamic and algal growth in a bubble column photobioreactor. In *Chem. Eng. Journal*, 229: 559-568

Nauha, E., K., Alopaeus, V. 2015. Modeling outdoors algal cultivation with compartmental approach. In *Chem. Eng. Journal*, 259: 945-960

Pilon, L., Berberoglu, H., Kandilian, R., 2011. Radiation transfer in photobiological carbon dioxide fixation and fuel production by microalgae. In *J. Quant. Spectrosc. Ra.*, 112(17): 2639-2660.

Pfleger, D., Becker, S., 2001. Modelling and simulation of the dynamic flow behavior in a bubble column. In *Chem. Eng. Sci.*, 56(4): 1737-1747.

Olivieri, G., Salatino, P., Marzocchella, A., 2014. Advances in photobioreactors for intensive microalgal production: configurations, operating strategies and applications. In *J. Chem. Technol. Biotechnol.*, 89: 178-195

Williams, P.J.le B., Laurens, L.M.L., 2010. Microalgae as biodiesel & biomass feedstocks: Review & analysis of the biochemistry, energetics & economics. In *Energy Environ. Sci.,* 3(5): 554-590.

Zhang, D., Dechatiwongse, P., Hellgardt, K., 2015. Modeling light transmission, cyanobacterial growth kinetics and fluid dynamics in a laboratory scale multiphase phot-bioreactor for biological hydrogen production", *Algal Research* 8, pp. 99-107.